Journal of Integrative Agriculture 2026, 25(9): 3736–3745

Available online at ScienceDirect

Journal of Integrative Agriculture

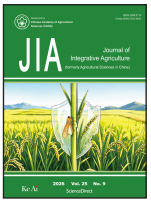

RESEARCH ARTICLE

A novel fucosylation-specific cell wall-degrading enzyme promotes *Magnaporthe oryzae* infection

Chang'an Ji, Zhao Hu, Yifang Zhang, Xia Song, Lei Su, Jintao Wang, Linxun Wu, Muxing Liu, Gang Li, Haifeng Zhang, Leiyun Yang, Xinyu Liu[#], Zhengguang Zhang[#]

State Key Laboratory of Agricultural and Forestry Biosecurity, Department of Plant Pathology, College of Plant Protection, Nanjing Agricultural University/ Key Laboratory of Integrated Management of Crop Diseases and Pests, Ministry of Education, Nanjing 210095, China

Highlights

- The α-L-fucosidase MoFco1 specifically hydrolyzes XXFG, an α-1,2-fucosylated xyloglucan oligosaccharide derived from plant hemicellulose.
- MoFco1 enzymatic activity is crucial for the full virulence of *Magnaporthe oryzae*.
- Compound 0989, identified through structure-based virtual screening, binds MoFco1 and significantly suppresses *M. oryzae* infection.

Abstract

Plant pathogenic fungi release cell wall-degrading enzymes (CWDEs), which are significant weapons for breaking down plant cell walls, although only a few reports focus on their pathogenesis. The current study demonstrates that MoFco1, a conserved α-L-fucosidase in several pathogenic fungi, degrades the hemicellulose component XXFG and contributes to the pathogenicity of *Magnaporthe oryzae*. In addition, MoFco1 enzyme activity is essential for its pathogenic function, as the enzyme activity mutation induced pathogenesis defects identical to the Δ*Mofco1* mutant. We further performed a structure-based virtual screening targeting MoFco1 and discovered 0989, which binds to MoFco1 and effectively inhibits *M. oryzae* pathogenesis. In brief, our study reveals the pathogenic mechanism of MoFco1 and explored the application of structure-based virtual screening in plant protection.

Keywords: *Magnaporthe oryzae*, α-L-fucosidase, cell wall-degrading enzyme, virtual screening

1. Introduction

Magnaporthe oryzae is the most devastating rice pathogen, causing 10–30% yield loss worldwide (Zhang *et al.* 2022). Current strategies primarily rely on resistant cultivars and fungicide applications (Skamnioti and Gurr 2009; Yang *et al.* 2024). However, continuous cultivation can quickly result in loss of resistance due to fungal adaptation and rapid genetic variation. Additionally, existing fungicides frequently lose efficacy as the fungus develops resistance to their targets (Khan *et al.* 2022; Li *et al.* 2023). Given the growing threat of rice blast disease and its enormous economic impact, there is an urgent need to develop novel fungicides with new targets.

The plant cell wall serves as a physical barrier that phytopathogenic fungi must cross to invade host tissues. Fungi produce various cell wall-degrading enzymes (CWDEs) that facilitate the degradation of plant cell wall components, enabling fungal penetration (Quoc and Nguyen 2017; Wan *et al.* 2021; Zhang *et al.* 2025). Various CWDEs, such as cellulose, hemicellulose, and pectinases, were identified during the interaction between rice and pathogens. These enzymes help digest the main structural polysaccharide components of the plant cell walls, allowing the pathogen to utilize these polysaccharides as nutrient sources (Fernandez *et al.* 2014). Despite the accumulated turgor pressure in the infection structure appressorium, which provides mechanical pressure to penetrate the host epidermis, CWDEs also play a critical role in breaching the plant cuticle and cell wall

Received 19 February 2025; Received in revised form 17 April 2025; Accepted 28 April 2025; Available online 2 June 2025
Chang'an Ji, E-mail: 2019202011@njau.edu.cn; [#]Correspondence Zhengguang Zhang, E-mail: zhgzhang@njau.edu.cn; Xinyu Liu, E-mail: xinyuliu@njau.edu.cn

doi: 10.1016/j.jia.2025.06.004

by hydrolyzing plant components, enabling *M. oryzae* to infect successfully. A genome-wide analysis of *M. oryzae* CWDEs revealed four distinct groups: cutinases, cellulases, hemicellulases, and pectinases (Quoc and Nguyen 2017). However, the pathogenic mechanism of CWDEs during *M. oryzae* infection needs further investigation.

With its diverse side-chain substitutions, hemicellulose is vital in plant responses to multiple external stressors (Grantham *et al.* 2017). Pathogenic fungi have developed hemicellulases to target various substrates, including α-L-fucosidases (Zhao *et al.* 2013). Previous studies show that FgFco1, an α-L-fucosidase from *Fusarium graminearum*, is active against XXFG, a fucose-side substitution of hemicellulose (Paper *et al.* 2013; Cao *et al.* 2014). However, its involvement in pathogenicity remains unclear.

Fucosylation is a biological process that occurs in vertebrates, invertebrates, plants, bacteria, and fungi and has been linked to mammalian physiological and pathological processes, including cell signaling and communication, tumor angiogenesis, immune system function, tumor cell migration and invasion, and cell-matrix interactions (Pan and Zhang 2025). The process is co-regulated by fucosyltransferases and fucosidases (Li *et al.* 2018). In mammals, α-1,6-fucosyltransferase (Fut8) is the sole enzyme responsible for core fucosylation, adding α-1,6-linked fucose to N-glycans (García-García *et al.* 2020; Pan and Zhang 2025). Loss of Fut8 causes defects in core fucosylation modification, resulting in growth retardation, emphysema, schizophrenia-like behavior, and even death (Lu *et al.* 2019; Pan and Zhang 2025). In plants, fucosylation occurs on various substrates, including pectin and xyloglucan (Schultink *et al.* 2014; Zhang *et al.* 2019). Defects in fucosylation inhibited the glycosylation of pattern-recognition receptors, affecting their ability to sense pathogen-associated molecular patterns (Zhang *et al.* 2019).

Our study identified an α-L-fucosidase MoFco1 (MGG_03257) in *M. oryzae*. We evaluated the function and pathogenicity of MoFco1 to determine whether it would be a viable target for fungicides. Furthermore, since small molecule inhibitor screening can target fungal virulence factors, we employed this technique to screen for MoFco1 targets that effectively suppress the rice blast. Our findings confirmed the significance of MoFco1 in *M. oryzae* pathogenesis and identified it as a promising fungicidal target.

2. Materials and methods

2.1. Fungal strains and media

Magnaporthe oryzae strain Guy11 was used as the wild-type strain (Qian *et al.* 2023). All strains were cultured on complete medium (CM) at 28°C (Talbot *et al.* 1993). Mycelia were collected from liquid CM for DNA, RNA, and protein extraction. Protoplasts were prepared and transformed as described previously (Sweigard *et al.* 1992). Transformants were selected on TB3 medium (3 g yeast extract, 3 g casamino acids, 200 g sucrose, and 7.5 g agar in 1 L distilled water) with 300 mg mL^{-1} hygromycin B (Roche, China) or 200 mg mL^{-1} zeocin (Invitrogen). For conidiation, strain blocks were maintained on straw decoction and corn (SDC) agar media at 28°C for 4 days in the dark followed by 3 days of constant illumination under fluorescent light (Hu *et al.* 2022; Qian *et al.* 2023).

2.2. Target gene deletion and complementation

The *MoFCO1* gene deletion mutant was obtained by the one-step gene replacement strategy. Sequence fragments located in the CDSs and upstream (1.0 kb) and downstream (0.8 kb) regions of target genes were amplified by PCR using the primer pairs listed in Appendix A. The resulting PCR products were recombined with hygromycin resistance cassette (HPH) by overlap PCR. The recombinant fragments were transformed into Guy11 protoplasts for mutation screening. Putative transformants were verified by PCR with the genomes. For complementation, the native promoter region and entire CDS were cloned by PCR and inserted into the pYF11 plasmid (bleomycin resistance) using the yeast XK125 (Bruno *et al.* 2004). The plasmids were introduced into protoplasts of the deletion mutants and screened by bleomycin resistance. The primer pairs were listed in Appendix A.

2.3. Functional appressorium detection

We harvested conidia and filtered them through two layers of Miracloth (EMD Millipore Corporation, 475855-1R, USA) with distilled water. For appressorium formation assays, droplets (30 μL) of conidial suspension were placed on hydrophobic coverslips (Fisher Scientific, Germany) under humid conditions at 28°C (Li *et al.* 2017). Appressorium turgor was measured using a 1–5 mol L^{-1} glycerol solution as described previously (Liu *et al.* 2016).

2.4. Plant materials and growth conditions

Rice (*Oryza sativa*) CO39 was used in this study. For experiments with seedlings, plants were grown in a growth chamber under the conditions of 16-h day, 28°C, 80% relative humidity (RH) followed by 8-h night, 26°C, 60% RH.

2.5. Infection and virulence assessment

For the virulence test of *M. oryzae*, conidia were suspended to a concentration of 5×10^4 spores mL^{-1} in a 0.2% (w/v) gelatin solution, and 4 mL each was sprayed on two-week-old rice CO39 seedlings (Ma *et al.* 2024).

To determine the activity of the compounds, the rice leaves were pretreated by the compounds 24 h in advance. Inoculated plants were kept in a growth chamber at 25°C with 90% humidity and in the dark for the first 24 h, followed by a 16 h/8 h light/dark cycle (Ma *et al.* 2024). The disease severity was assessed at 7 days post inoculation. The concentration of 0104/0989/1432 was 0.1 mmol L^{-1}, 1% DMSO as control.

For observation of the penetration and invasive growth in plant cells, conidial suspensions (5×10^4 spores mL^{-1}) were injected into the rice leaf sheath At 28°C for 36 h, the inner epidermis of infected sheaths was observed under confocal microscope. Confocal microscopy was performed using a ZEISS LSM 980 microscope (Zeiss, Oberkochen, Germany) equipped with Airyscan2 system. Excitation/emission wavelengths were 488/505 nm for EGFP. Images were acquired and processed using LSM980 ZEN 3.3 software (Zeiss, Oberkochen, Germany).

2.6. Reactive oxygen species (ROS) observation

To observe ROS derived from rice, the rice leaf sheaths were stained with DAB (Sigma-Aldrich, China) as previously described (Hu *et al.* 2022).

2.7. RNA isolation and qRT-PCR

For quantification of gene expression, RNA was isolated by Ultrapure RNA Kit (CW0581S, CWBIO, China). cDNA synthesis was performed by PrimeScript™ RT Reagent Kit (TaKaRa, Japan). Quantitative RT-PCR was performed with the 7500 Fast Real-Time System (ABI, USA), and transcripts were analyzed by the 7500 System SDS software. To compare the relative abundance of PR genes transcripts, the average threshold cycle (Ct) was normalized to rice actin for each of the treated samples. The primer pairs were listed in Appendix A.

2.8. Enzyme activity assay

2′-Fucosyllactose (2′-FL) was purchased from MCE (Med Chem Express, China). XXFG oligosaccharide was purchased from Elicityl (France). 2′-FL and XXFG were dissolved in 25 mmol L^{-1} sodium acetate, pH 5.0, at a concentration of 10 mg mL^{-1}. Each assay contains 10 μL of 10 mg mL^{-1} 2′-fucosyllactose or XXFG, 2 μg of enzyme (or buffer control), and 50 mmol L^{-1} sodium acetate (pH 5.0). The total volume of 100 μL in each assay was made up by 50 mmol L^{-1} sodium acetate. The assays were performed at 37°C for 12 h. L-Fucose Assay Kit (Megazyme, Ireland) was used to detect the production of L-fucose.

2.9. Microscale thermophoresis (MST) analysis

Binding reactions of MoFco1 and its interaction sites mutation proteins with compounds were measured by MST in a Monolith NT.Label Free (Nano Temper Technologies GMBH, Monolish NT.115, China) instrument. Labeled proteins (10 μmol L^{-1}) were displaced by a buffer. A range of concentrations of compounds in the assay buffer was incubated with labeled protein (1:1, v/v) for 10 min. The analysis is performed using the Nano Temper Analysis software (version 1.5.41) (Hu *et al.* 2022).

2.10. Virtual screening

According to the physical properties and molecular weight, the structure files of compounds were downloaded from compound databases such as ZINC and PubChem. Use OpenBabel and AutoDockTools to process the structure file and generate a pdbqt format file that can be used for docking. Use AutoDockTools to process the protein structure file and obtain the size and coordinate parameters of the docking box. Use AutoDock Vina to perform molecular docking and save the docking results in a new file. Sort according to the size of the affinity, and select appropriate compounds for next experiments. Use Python scripts to drive batch processing of the above processes.

3. Results

3.1. Identification of MoFco1 in *M. oryzae*

To identify α-L-fucosidase homologs in *M. oryzae*, we constructed a phylogenetic tree based on the α-L-fucosidase ortholog group (OG6_102401) from FungiDB. The analysis revealed two distinct subfamilies of fungi α-L-fucosidases (Fig. 1-A). Within these subfamilies, we identified three putative α-L-fucosidases in *M. oryzae*, including MGG_03257, MGG_00316, and MGG_00042 (Fig. 1-A). Our analysis also placed previously reported protein, FgFco1 in these subfamilies (Fig. 1-A). Further examination of conserved domains combined with Pfam data indicated that members of subfamily 2, such as MGG_03257, consistently harbor both the α-L-fucosidase (α-L-fucos) and C-terminal (Fucosidase_C) domains. In contrast, subfamily 1 members, including MGG_00316 and MGG_00042, primarily feature only the α-L-fucos domain (Fig. 1-B).

Sequence alignment between *M. oryzae* α-L-fucosidases and FgFco1 revealed that MGG_03257 exhibited substantial homology to FgFco1 with 96% coverage and 64.82% identity (Appendix B). This result suggests that MGG_03257 is highly conserved regarding sequence and potential function. Therefore, MGG_03257 was renamed MoFco1 and further investigated for its role in the interaction with rice. MGG_00042 and MGG_00316, belonging to subfamily 1, were less similar to FgFco1, with sequence alignments showing 61% and 73% coverage, and identities of 26.75% and 24.74%, respectively (Appendix B). In addition, the structural alignment of MoFco1 and FgFco1 yielded a root mean square deviation (RMSD) of 0.441 (Appendix C), suggesting that these two proteins are structurally comparable and functionally conserved.

3.2. MoFco1 catalyzes the hydrolysis of α-1,2 linked fucose residues

We next investigated the catalytic properties of MoFco1, specifically its ability to hydrolyze α-1,2 linked fucose residues. Using L-fucose as a ligand, we performed docking studies with AutoDock Vina. We identified six critical residues (LYS288, ASP242, HIS143, TRP327, GLU61, and TRP62) involved in MoFco1's enzymatic activity (Fig. 2-A). To validate the role of these residues, we generated a mutant variant of MoFco1, MoFco1^{6A}, which had these six residues substituted. We measured the release of L-fucose from 2′-FL at 340 nm to evaluate the enzymatic activity of both wild-type MoFco1 and MoFco1^{6A}, building on prior research using 2′-FL, the most prevalent human milk oligosaccharide (HMO) containing α-1,2-linked fucose. The results demonstrated that wild-type MoFco1 could hydrolyze α-1,2-linked fucose residues. In contrast, the MoFco1^{6A} mutant exhibited significantly reduced enzyme activity (Fig. 2-B). Furthermore, in line with earlier research on FgFco1, we investigated MoFco1's efficacy against XXFG, the oligosaccharide component of hemicellulose. Our findings revealed that MoFco1 is also active against XXFG (Fig. 2-C).

3.3. MoFco1 localizes in the extra-invasive hyphal membrane (EIHM)

Given that XXFG is a crucial cell wall component, we hypothesized that MoFco1 is secreted into the extracellular

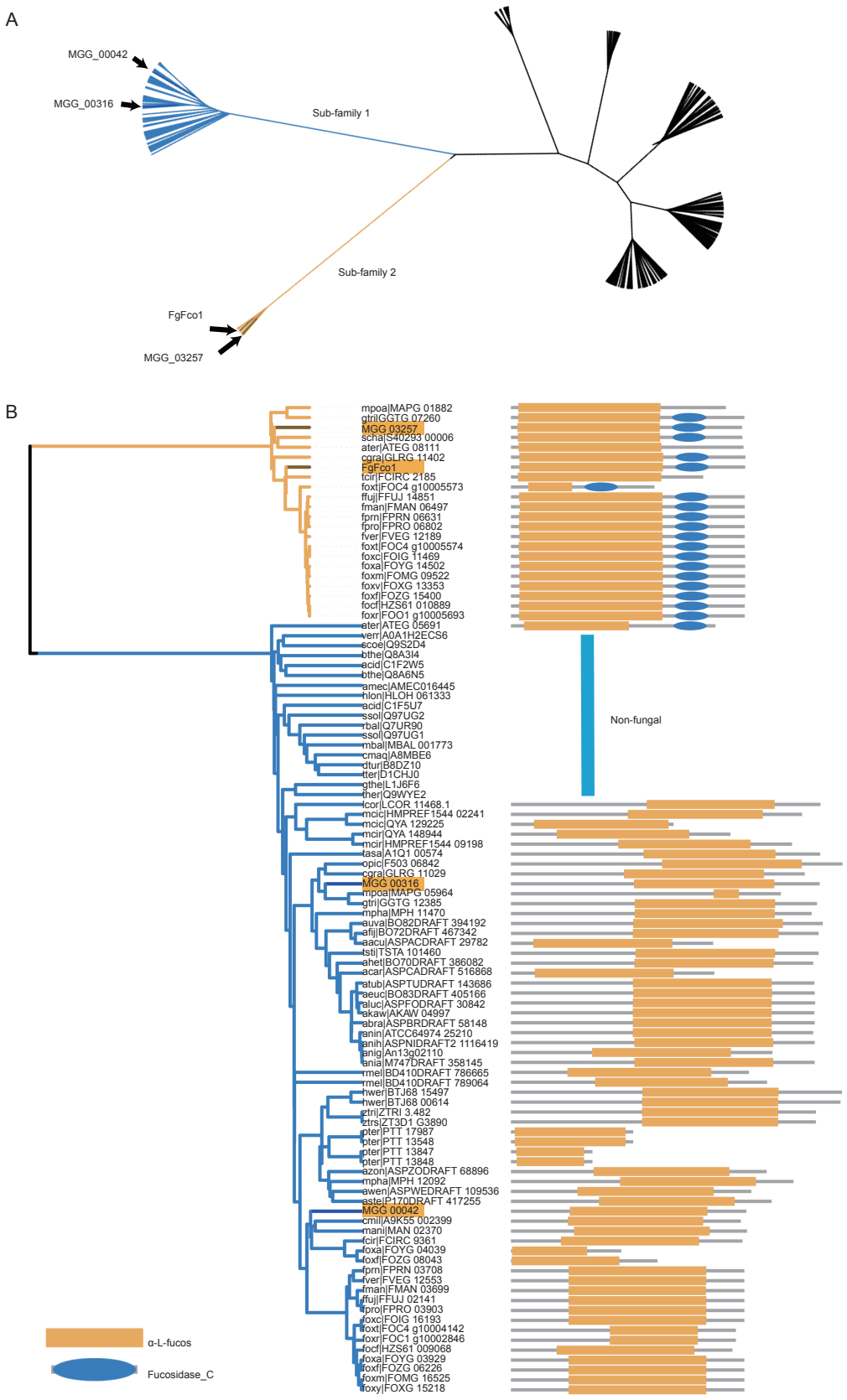

Fig. 1 MoFco1 belongs to subfamily 2. A, the evolutionary tree featuring MoFco1. The evolutionary tree displays the sequence alignment of MoFco1 and putative α-fucosidases from other organisms (OG6_102401, 368 sequences satisfied with E-value<1e–5 and percent match length≥50% from 800 species). Subfamily 2 branches are colored in yellow, whereas subfamily 1 branches are colored in blue. B, an evolutionary tree with Pfam domain analysis. It demonstrates the disparity in domain conservation between the two subfamilies. Subfamily 2 branches are shown in yellow. A yellow rectangle highlights the α-fucosidase domain (α-L-fucos), while the α-fucosidase C-terminal domain (Fucosidase_C) is shown in a blue oval.

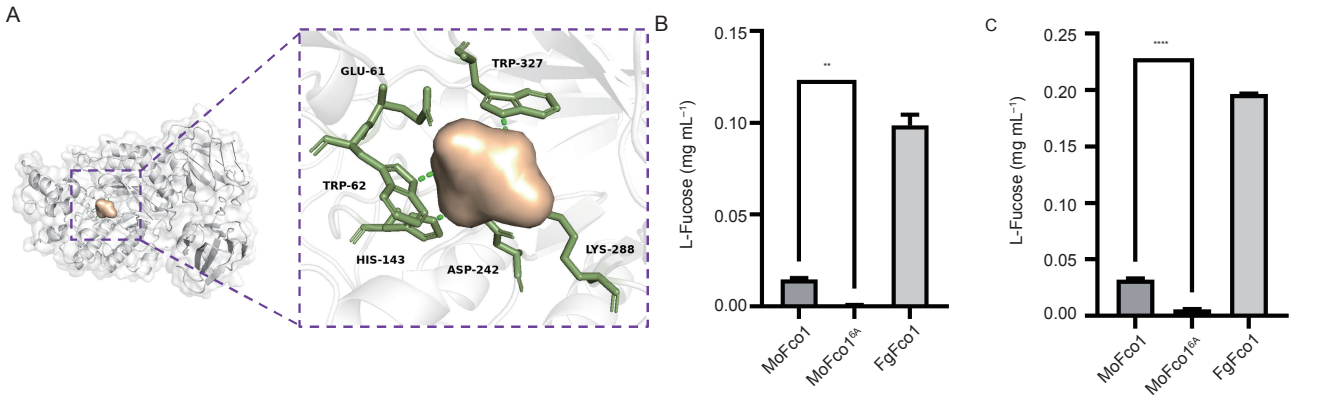

Fig. 2 MoFco1 targets α-1,2 fucose. A, six critical residues involved in the enzymatic activity of MoFco1. B, enzyme activity assay of MoFco1 and MoFco1^{6A} based on 2′-FL. C, enzyme activity assay of MoFco1 and MoFco1^{6A} based on XXFG. Ordinary one-way ANOVA, error bars are standard deviation. **, P<0.01; ****, P<0.0001.

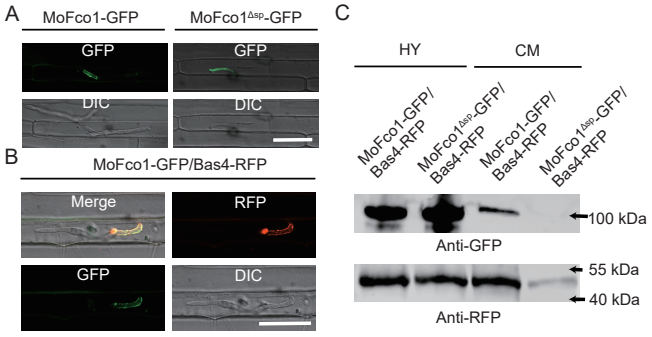

Fig. 3 MoFco1 is localized at EIHM. A, MoFco1's localization during the infection stage. A Δ*Mofco1* transformant expressing both MoFco1-GFP and Bas4-RFP was used to visualize the cellular localization of MoFco1 and the apoplastic effector Bas4 in planta. At 24 h post-inoculation (hpi), the MoFco1-GFP signal enclosed IH and co-localized with Bas4-RFP. Scale bars measure 10 mm. B, localization of MoFco1 and MoFco1$^{\Delta SP}$ during the infection stage. Images were examined using a confocal microscope at 24 hpi. Scale bar measures 10 μm. C, detection of MoFco1 secreted into CM. Proteins were enriched from the CM medium and mycelium. The presence of GFP-tagged proteins was determined by Western blotting using an anti-GFP tag antibody.

space and interacts with the rice cell wall components. We thus generated a Δ*Mofco1* mutant strain and created strains (Δ*Mofco1*/*MoFCO1-GFP* and Δ*Mofco1*/*MoFCO1*$^{\Delta SP}$*-GFP*) to study MoFco1 secretion in EIHMs. After inoculating rice leaf sheaths with the strains, the inner epidermal cells of the infected sheaths were evaluated using laser scanning confocal microscopy (ZEISS LSM 980 with Airyscan2) 24 h later. We detected fluorescence around the penetration peg in the infected rice sheath cells. *Magnaporthe oryzae* infected rice sheath cells showed MoFco1$^{\Delta SP}$-GFP localization in the cytoplasm and MoFco1-GFP localization in the apoplast (Fig. 3-A). To further confirm the localization of MoFco1, we expressed Bas4-RFP, an apoplastic effector that resides in EIHM, in Δ*Mofco1*/*MoFCO1-GFP* strain. The co-localization of MoFco1 and Bas4 at the EIHM confirmed the secretion of MoFco1 into the EIHM (Fig. 3-B).

We isolated the extracellular fluid from rice that had been inoculated with the MoFco1-GFP strain for 48 h to ascertain the localization of MoFco1 during infection. We then enriched the extracellular fluid with anti-GFP nanobody agarose beads and detected the presence of MoFco1 in the apoplast (Appendix D). The MoFco1-GFP strain showed a distinct protein band in its culture media, while the MoFco1$^{\Delta SP}$-GFP strain (which lacks the signal peptide of MoFco1) did not (Fig. 3-C). These findings indicated that MoFco1 functions as a putative apoplastic effector.

3.4. *Magnaporthe oryzae* requires the presence of MoFco1 to be fully virulent

Given that MoFco1 is secreted into the apoplastic space and functions as a hydrolase for rice cell wall components, it is plausible that it is essential for *M. oryzae*'s full virulence. We assessed its growth, conidiation, and appressorium formation. We measured the colony diameter of Guy11, Δ*Mofco1*, and Δ*Mofco1*/*MoFCO1* strains cultured on CM (complete medium) and MM (minimal medium) media (Appendix E). We also quantified conidiation on the SDC medium and assessed turgor pressure in appressoria (Appendix E). These phenotypes of the Δ*Mofco1* mutant and wild-type strain showed no significant differences.

We first tested the Δ*Mofco1* mutant on barley leaves to assess its role in pathogenicity and found that its virulence was markedly reduced (Appendix E). Then, we sprayed Guy11, Δ*Mofco1*, and Δ*Mofco1*/*MoFCO1* conidial suspensions onto CO39 rice seedlings (susceptible cultivar) to test virulence. Δ*Mofco1*-infected leaves showed reduced and restricted lesion formation, highlighting the significance of MoFco1 for full virulence in *M. oryzae*. In addition, the enzymatic activity-deficient strain Δ*Mofco1*/*MoFCO1*^{6A}*-GFP* exhibited deficits in pathogenicity on rice, similar to the Δ*Mofco1* mutant strains (Fig. 4-A–C). The pathogenicity test in rice leaf sheaths also showed the pathogenicity decrease in Δ*Mofco1* and Δ*Mofco1*/*MoFCO1*^{6A} strains (Fig. 4-D). These results demonstrate that the enzymatic activity of MoFco1 is essential for the full virulence of *M. oryzae*.

We also conducted an infection assay on rice sheath to further evaluate the role of MoFco1 in host colonization. At 36 h post-inoculation (hpi), we detected the appearance of

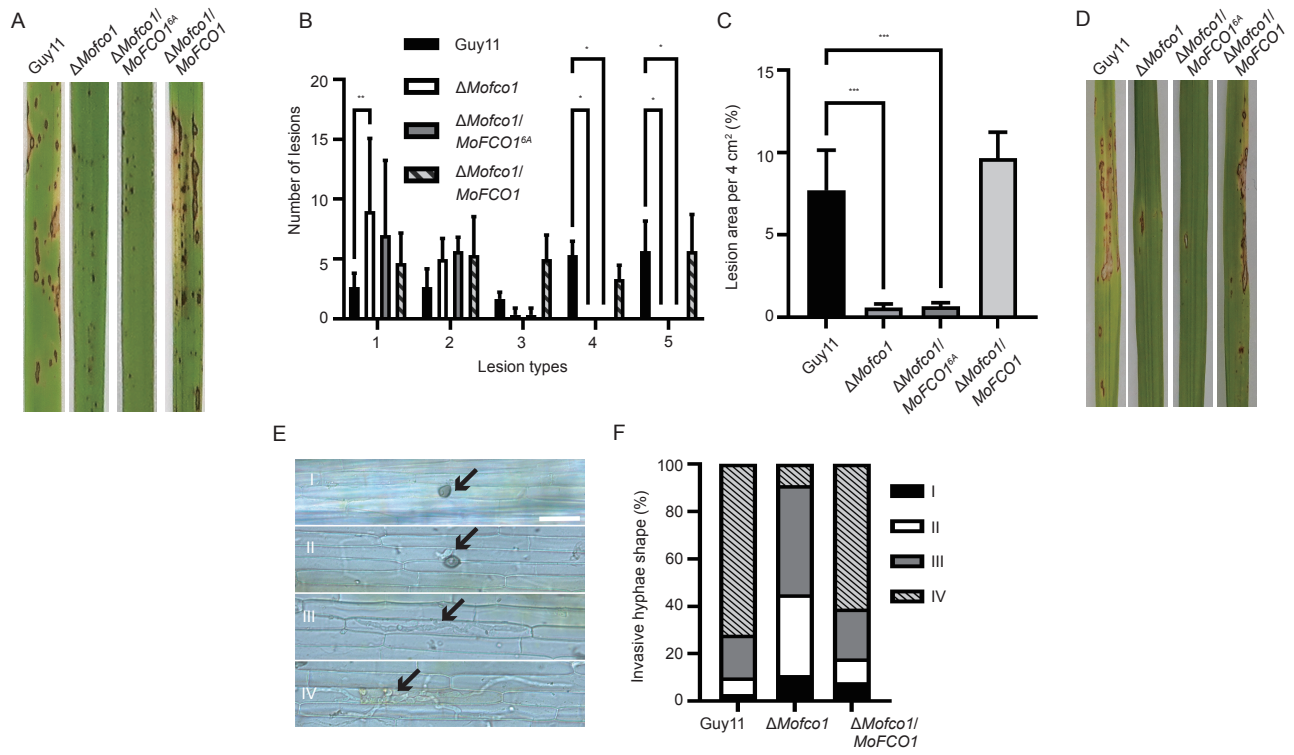

Fig. 4 MoFco1 is required for pathogenicity. A, pathogenicity test on rice leaves. It shows the reduction in pathogenicity of Δ*Mofco1* and Δ*Mofco1*/*MoFCO1*^{6A}. Four milliliters of conidial suspension (5×10^4 spores mL^{-1}) of Guy11, Δ*Mofco1*, Δ*Mofco1*/*MoFCO1*^{6A}, Δ*Mofco1*/*MoFCO1* were sprayed on *Oryza sativa* cv. CO39 and photographed 7 days post-inoculation (dpi). B, quantification of lesion types. Type 0, no visible evidence of infection; type 1, uniformly dark brown pinpoint lesions without visible centers; type 2, small lesions with distinct tan centers surrounded by a darker brown margin; type 3, small eyespot lesions approximately 2 mm in length with tan centers surrounded by dark brown margins; type 4, intermediate size eyespot lesions, approximately 3-4 mm in length; and type 5, large eyespot lesions that attain the maximum size seen for a particular cultivar. Lesions were photographed and measured at 7 dpi, and lesion numbers within an area of 4 cm^2 were counted. Two-way ANOVA, error bars are standard deviation. *, P<0.05; **, P<0.01. C, assessment of the lesion area using ImageJ. Ordinary one-way ANOVA, error bars are standard deviation. ***, P<0.001. D, pathogenicity test in rice leaf sheaths. Conidial suspension (3×10^5 spores mL^{-1}) of Guy11, Δ*Mofco1*, Δ*Mofco1*/*MoFCO1*^{6A}, Δ*Mofco1*/*MoFCO1* were injected into leaf sheaths of CO39 and photographed 5 dpi. E and F, statistical analysis of invasive hyphae shape. Invasive hyphae were classified into four types: I, appressorium without penetration peg; II, appressorium with primary invasive hyphae; III, secondary invasive hyphae that do not extend to neighboring plant cells; and IV, invasive hyphae that extend into surrounding plant cells. Arrows show the invasive hyphae shape in different types. Scale bar measures 10 μm.

invasive hyphae (IH) at 100 appressorium penetration sites. Hyphal growth could be classified into four types: type I (no penetration), type II (primary IH present), type III (secondary IH does not extend to neighboring plant cells), and type IV (IH extends into neighboring plant cells). At 36 hpi, more than 80% of penetration sites in the WT and complemented strains exhibited type III and IV growth. In contrast, the Δ*Mofco1* mutant showed significantly reduced IH invasion, with only 55% of penetration sites expressing type III and IV growth (Fig. 4-E and F). These results demonstrate that MoFco1 is essential for proper IH development and host colonization.

3.5. MoFco1 suppresses host defense responses

To further investigate MoFco1's role in fungal pathogenicity, we examined its response to oxidative stress induced by Diamide treatment. The results showed that Δ*Mofco1* mutant exhibited significant inhibition under diamide treatment (Appendix F). We used DAB staining to quantify ROS levels in Guy11, Δ*Mofco1*, Δ*Mofco1*/*MoFCO1*^{6A}-*GFP*, and Δ*Mofco1*/*MoFCO1-GFP* strains during infection on rice cells, evaluating host-derived ROS generation *in vivo*. The Δ*Mofco1* mutant or its enzymatic activity-deficient strain showed enhanced ROS accumulation than the wild-type strain Guy11 and the complemented strains Δ*Mofco1*/*MoFCO1-GFP* (Fig. 5-A and B). Exogenously applying DPI, an NADPH oxidase inhibitor, to the rice sheath during infection restored the infection defects observed in the Δ*Mofco1* mutant (Fig. 5-C). Furthermore, the expression of *MoFCO1* during different infection stages was analyzed by qRT-PCR. The result shows that *MoFCO1* is highly upregulated at 24 hpi (Fig. 5-D). To further investigate the impact of *MoFCO1* on host defense, we then analyzed the expression of several defense-related genes in rice at 3 and 24 hpi by qRT-PCR. At 24 hpi, the expression of *CRT1* and *NPR1* are significantly increased in Δ*Mofco1* and Δ*Mofco1*/*MoFCO1*^{6A} mutants when compared to the wild-type (Fig. 5-E and F; Appendices G and H). These findings indicate that MoFco1 plays a crucial role in mitigating oxidative stress and suppressing host defense responses during infection.

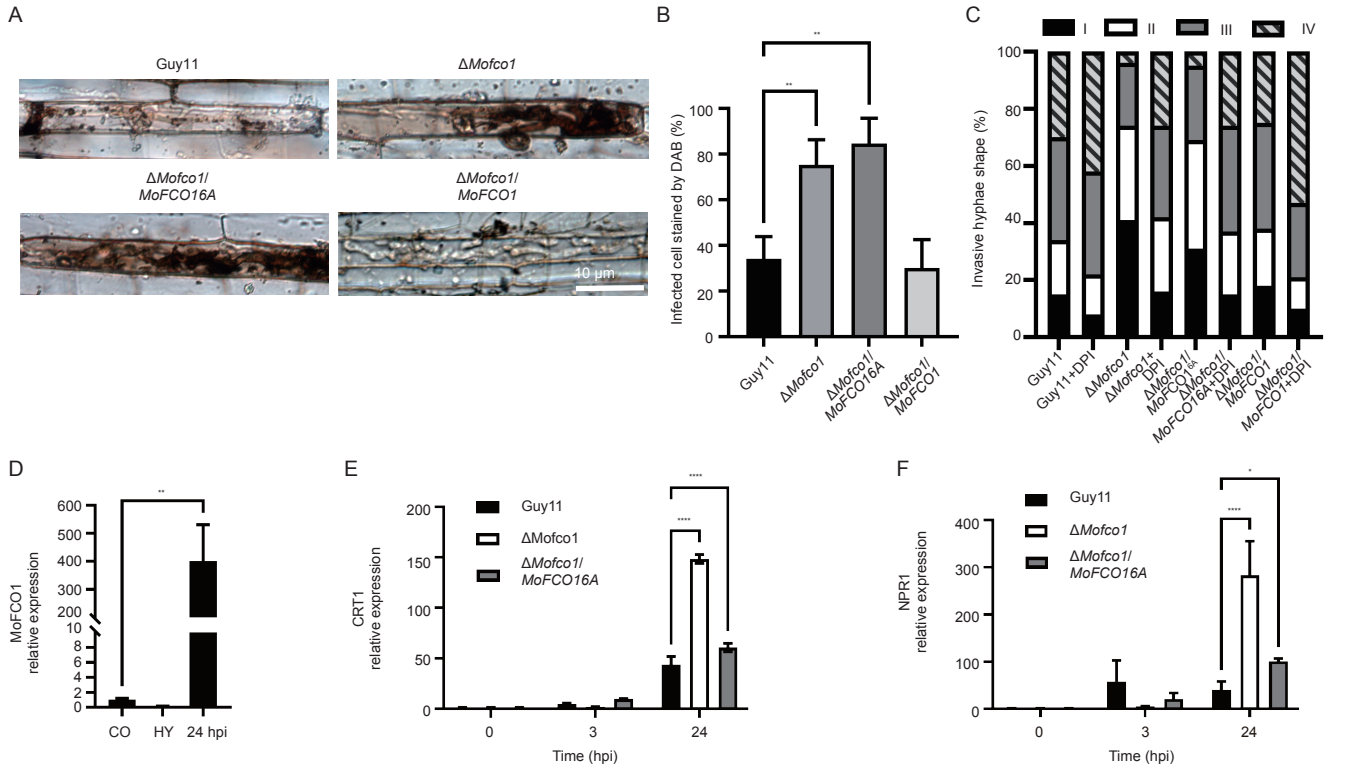

Fig. 5 MoFco1 suppresses host defense responses. A and B, the inability of the Δ*Mofco1* mutant to inhibit the reactive oxygen species (ROS) burst in rice cells. DAB staining was performed on infected CO39 leaf sheath with Guy11, Δ*Mofco1*, Δ*Mofco1*/*MoFCO1*^{6A}, and Δ*Mofco1*/*MoFCO1* at 36 h post-inoculation (hpi). The graphics depict the number of appressoria (*n*=100) that induce H_2O_2 in the rice cells invaded by invasive hyphae (IH). Scale bar measures 10 μm. Ordinary one-way ANOVA, error bars are standard deviation. **, *P*<0.01. C, statistical analysis of invasive hyphae classified into four types. Statistical analysis was performed on the IH types of Guy11, Δ*Mofco1*, and Δ*Mofco1*/*MoFCO1*^{6A} with or without 500 nmol L^{-1} DPI (diphenyleneiodonium) at 24 h. D, relative mRNA expression of *MoFCO1* at 24 hpi with Guy11 on CO39 by qRT-PCR. Ordinary one-way ANOVA, error bars are standard deviation. **, *P*<0.01. E, relative mRNA expression of *CRT1* at 3 and 24 hpi with Guy11, Δ*Mofco1*, and Δ*Mofco1*/*MoFCO1*^{6A} on CO39 by qRT-PCR. F, relative mRNA expression of *NPR1* at 3 and 24 hpi with Guy11, Δ*Mofco1*, and Δ*Mofco1*/*MoFCO1*^{6A} on CO39 by qRT-PCR. Two-way ANOVA, error bars are standard deviation. *, *P*<0.05; ****, *P*<0.0001.

3.6. 0989 effectively inhibits the pathogenicity of *M. oryzae*

The significance of fucosylation and α-L-fucosidases in cellular processes has led to the development of small molecule inhibitors that target α-L-fucosidases in human diseases (Miura *et al.* 2019). Structure-based molecular docking of proteins and small molecules (<1,000 Da, primarily <400 Da) is broadly used to develop human therapeutic drugs (Li *et al.* 2013). However, it has been rarely utilized to identify fungicides for crop protection. This study screened lead-like compounds from the ZINC Database as potential ligands for MoFco1. OpenBabel was used to transform file formats, AutoDockTools to configure parameters, and AutoDock Vina with Python scripts to run docking simulations. Following a ranking based on binding affinity, three ligands (1432, 0989, and 0104) with the lowest binding affinities were chosen for further analysis. The interactions between these ligands and MoFco1 were visualized and analyzed using PyMOL (Fig. 6-A–C). Rice plants were treated with each ligand for 24 h before being inoculated with the Guy11 strain to assess their efficacy. Among these ligands, 0989 treatment significantly reduced pathogenicity, comparable to MoFco1 deletion. In contrast, 0104 showed little effect on *M. oryzae* infection, while 1432 caused leaf death in rice plants (Appendix I). These results suggested that 0989 is an effective inhibitor capable of lowering *M. oryzae* pathogenicity (Fig. 6-D). MST validated the interaction between MoFco1 and 0989, indicating that 0989 functions as a selective inhibitor of MoFco1 (Fig. 6-E and F; Appendix J).

4. Discussion

The plant cell wall is a dynamic and complex structure essential for growth, development, and protection against numerous biotic and abiotic stresses (Levesque-Tremblay *et al.* 2015; Baez and Bacete 2023). Fucosylation, a typical hemicellulose side-chain modification, is pivotal in modulating plant responses to external stresses (Li *et al.* 2018). For example, the degree of fucosylation of xyloglucan, the predominant hemicellulosic polysaccharide in primary plant cell walls, affects the Al binding capacity of hemicellulose (Wan *et al.* 2018). Fucosylation plays a key role in plant immunological responses, including pattern-triggered immunity (PTI) and effector-triggered immunity (ETI) (Zhang *et al.* 2019). Our study identified the α-L-fucosidase MoFco1 of *M. oryzae* and revealed that its enzymatic activity

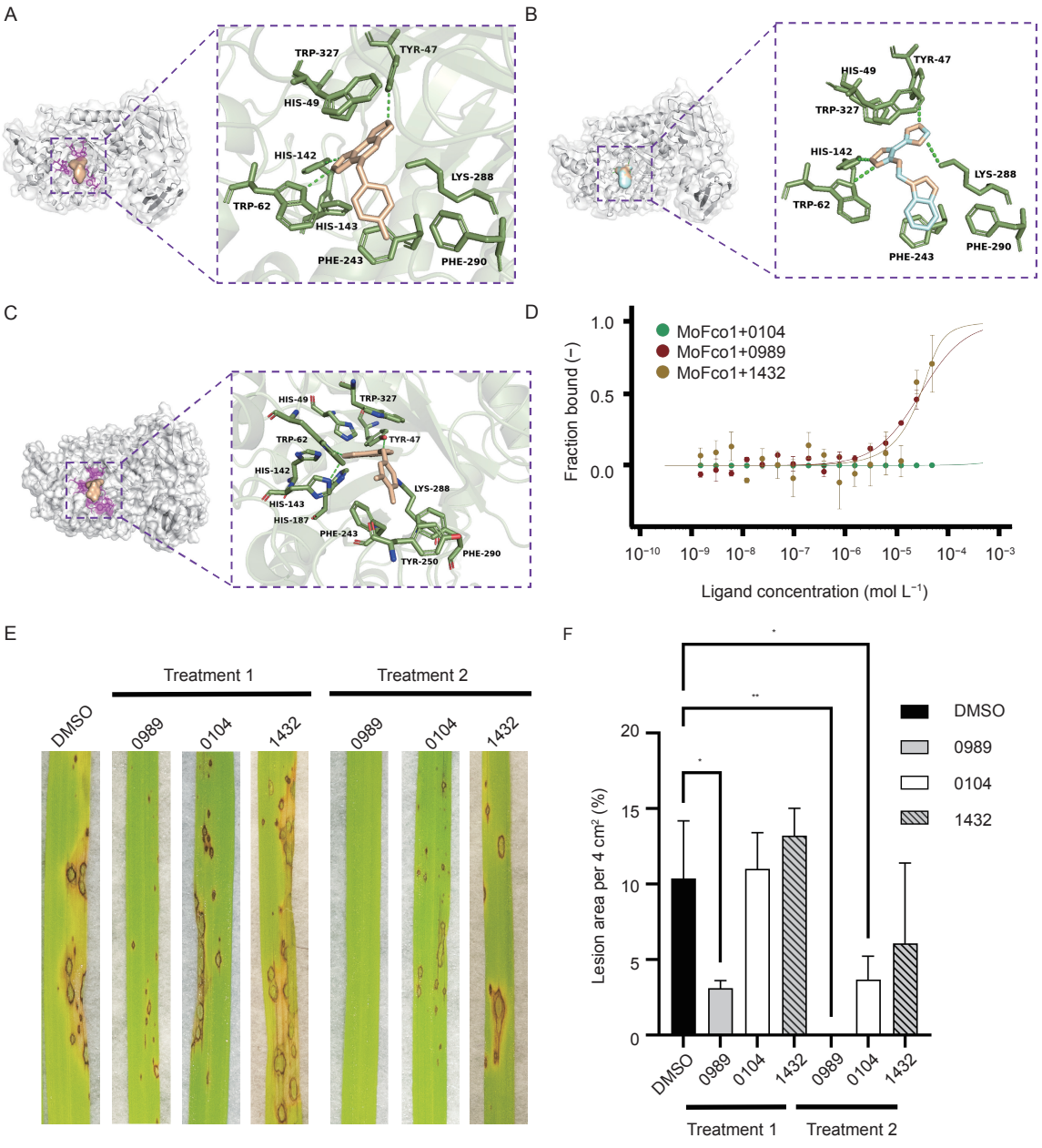

Fig. 6 MoFco1 binds the inhibitor 0989. A, the docking of MoFco1 and 0989. B, the docking of MoFco1 and 0104. C, the docking of MoFco1 and 1432. D, evaluation of the three compounds using microscale thermophoresis (MST). MoFco1 was labeled by RED-NHS. The raw data were integrated and fitted to a binding model using the MST analysis software. The recombinant proteins were expressed in *Pichia pastoris* using the pPIC9k vector. E, pathogenicity test of the three compounds on rice leaves. Treatment 1, the compounds were treated 24 h before the spores; treatment 2, the compounds and spores were treated at the same time. F, assessment of the lesion area using ImageJ. Ordinary one-way ANOVA, error bars are standard deviation. *, $P<0.05$; **, $P<0.01$.

determines its function in pathogenesis. Mutations in the enzyme's active sites significantly reduced the pathogen's ability to cause infection.

Monosaccharides produced by CWDEs serve as a nutritional source for plant pathogens (Gibson *et al.* 2011). Unlike other monosaccharides like trehalose, which *M. oryzae* can synthesize, L-fucose can only be absorbed from the apoplast (Goldman *et al.* 2013; Cai *et al.* 2018). The current study discovered that fucosylation mostly depends on the function of fucosyltransferase, whose substrate is GDP-L-fucose (Becker and Lowe 2003). GDP-L-fucose is synthesized using both the *de novo* and salvage pathways (Wang *et al.* 2009). We searched the *M. oryzae* database for homologous proteins of these two pathway-related proteins based on their protein sequence similarity and discovered no matches using local BlastP. Nevertheless, except five putative α-L-fucosidases, we identified three putative fucose-related proteins in *M. oryzae*, including L-fucose-proton symporter (MGG_09193), L-fucose permease glucose/galactose transporter (MGG_00846), and uncharacterized fucose permease (MGG_01811). These genes are involved in the transmembrane transport of L-fucose, implying that

L-fucose is sourced externally in *M. oryzae*. The degree of fucosylation determines the susceptibility of plant cell walls to pathogen infection. Reduced fucosylation in *Arabidopsis* causes several impairments, including defects in stomatal and apoplast defense, glycosylation of pattern recognition receptors, and responses mediated by PTI and ETI (Wan *et al.* 2018). Thus, *M. oryzae* targets rice cell wall fucosylation by secreting MoFco1, acquiring external L-fucose, and inhibiting the plant's defenses during infection.

Our findings suggest that targeting CWDEs with inhibitors is a viable strategy for managing plant pathogens. Previous research has shown that the evolutionarily conserved *M. oryzae* effector MoErs1 is a fungicidal target. In *Phytophthora sojae*, chitin synthases, whose catalytic mechanism is well understood, are important therapeutic targets. Thus, the target should feature a highly conserved structure and a defined catalytic mechanism. In contrast to effectors, which constantly evolve in the arms race between plants and pathogens (Wang *et al.* 2017), the enzymatic active centers of CWDEs are preserved due to substrate specificity. We identified evolutionary conserved CWDEs and used docking to determine active sites associated with enzymatic activity to screen for potential inhibitors.

Artificial intelligence-assisted virtual screening is a powerful approach for detecting plant pathogen inhibitors. Virtual screening provides a cost-effective alternative to conventional high-throughput screening (HTS) in identifying bioactive compounds (Blay *et al.* 2020). This approach has been utilized in plant pathogen research, including the identification of inhibitors that target the uridyltransferase activity of *Xanthomonas oryzae* pv. *oryzae* GlmU (Min *et al.* 2012) and enzymes involved in the trehalose biosynthesis pathway in *M. oryzae* (Chen *et al.* 2024). Studies on catalytic mechanisms and docking necessitate the elucidation of precise protein structures. Previously, protein structures were generated using protein crystallization (Min *et al.* 2012). However, advances in artificial intelligence, including tools like AlphaFold, now provide high-confidence predictions of most protein structures (Liu *et al.* 2024; Mall *et al.* 2025). Thus, drug discovery is accelerated by artificial intelligence and precise forecasting (Jumper *et al.* 2021).

Furthermore, artificial intelligence extends beyond protein structure prediction to include other aspects of drug discovery. For example, the primary application of AlphaFold3 is to unravel mechanisms by analyzing molecular interactions, including proteins-proteins and proteins-compounds. AlphaFold has been used to redesign an inhibitor for broad-spectrum disease resistance (Homma *et al.* 2023) and to drive the development of a fusion enzyme to improve biosynthesis. Thus, artificial intelligence-assisted virtual screening will find numerous applications in developing pathogenic fungal inhibitors. The artificial intelligence-assisted virtual screening used in the present study could be helpful in the prevention and control of rice blasts.

Acknowledgements

This research was supported by the National Key Research and Development Program of China (2022YFD1700200), the Young Elite Scientists Sponsorship Program by CAST (2022QNRC001), the Natural Science Foundation of China (NSFC) (32272496, 32293241 and 32293245). Virtual screening supported by the high-performance computing platform of Bioinformatics Center, Nanjing Agricultural University.

Declaration of competing interest

The authors declare that they have no conflict of interest.

Declaration of generative AI and AI-assisted technologies in the writing process

During the preparation of this manuscript, the authors used Deepseek to assist in improving the clarity and readability of the language. All content generated was carefully reviewed and revised by the authors as necessary, and the authors take full responsibility for the final content of the article.

Appendices associated with this paper are available at https://doi.org/10.1016/j.jia.2025.06.004

References

Baez L A, Bacete L. 2023. Cell wall dynamics: Novel tools and research questions. *Journal of Experimental Botany*, **74**, 6448–6467.

Becker D J, Lowe J B. 2003. Fucose: Biosynthesis and biological function in mammals. *Glycobiology*, **13**, 41R–53R.

Blay V, Tolani B, Ho S P, Arkin M R. 2020. High-throughput screening: Today's biochemical and cell-based approaches. *Drug Discovery Today*, **25**, 1807–1821.

Bruno K S, Tenjo F, Li L, Hamer J E, Xu J R. 2004. Cellular localization and role of kinase activity of PMK1 in *Magnaporthe grisea*. *Eukaryotic Cell*, **3**, 1525–1532.

Cao H, Walton J D, Brumm P, Phillips Jr G N. 2014. Structure and substrate specificity of a eukaryotic fucosidase from *Fusarium graminearum*. *Journal of Biological Chemistry*, **289**, 25624–25638.

Cai X, Seitl I, Mu W, Zhang T, Stressler T, Fischer L, Jiang B. 2018. Biotechnical production of trehalose through the trehalose synthase pathway: Current status and future prospects. *Applied Microbiology and Biotechnology*, **102**, 2965–2976.

Chen Y, Tang L, Jiang Z, Wang S, Qi L, Tian X, Deng H, Kong Z, Gao W, Zhang X, Li S, Chen M, Zhang X, Duan H, Yang J, Peng Y L, Wang D, Liu J. 2024. Dual-specificity inhibitor targets enzymes of the trehalose biosynthesis pathway. *Journal of Agricultural and Food Chemistry*, **72**, 209–218.

Fernandez J, Marroquin-Guzman M, Wilson R A. 2014. Mechanisms of nutrient acquisition and utilization during fungal infections of leaves. *Annual Review of Phytopathology*, **52**,155–174.

García-García A, Ceballos-Laita L, Serna S, Artschwager R, Reichardt N C, Corzana F, Hurtado-Guerrero R. 2020. Structural basis for substrate specificity and catalysis of α1,6-fucosyltransferase. *Nature Communications*, **11**, 973.

Gibson D M, King B C, Hayes M L, Bergstrom G C. 2011. Plant pathogens as a source of diverse enzymes for lignocellulose digestion. *Current Opinion in Microbiology*, **14**, 264–270.

Goldman W E, Tournu H, Fiori A, Van Dijck P. 2013. Relevance of trehalose in pathogenicity: Some general rules, yet many exceptions. *PLoS Pathogens*, **9**, e1003447.

Grantham N J, Wurman-Rodrich J, Terrett O M, Lyczakowski J J, Stott K, Iuga D, Simmons T J, Durand-Tardif M, Brown S P, Dupree R, Busse-Wicher M, Dupree P. 2017. An even pattern of xylan substitution is critical for interaction with cellulose in plant cell walls. *Nature Plants*, **3**, 859–865.

Homma F, Huang J, van der Hoorn R A L. 2023. AlphaFold-Multimer predicts cross-kingdom interactions at the plant-pathogen interface. *Nature Communications*, **14**, 6040.

Hu J, Liu M, Zhang A, Dai Y, Chen W, Chen F, Wang W, Shen D, Telebanco-Yanoria MJ, Ren B, Zhang H, Zhou H, Zhou B, Wang

P, Zhang Z. 2022. Co-evolved plant and blast fungus ascorbate oxidases orchestrate the redox state of host apoplast to modulate rice immunity. *Molecular Plant*, **15**, 1347–1366.
Jumper J, Evans R, Pritzel A, Green T, Figurnov M, Ronneberger O, Tunyasuvunakool K, Bates R, Žídek A, Potapenko A, Bridgland A, Meyer C, Kohl S A A, Ballard A J, Cowie A, Romera-Paredes B, Nikolov S, Jain R, Adler J, Back T, *et al*. 2021. Highly accurate protein structure prediction with AlphaFold. *Nature*, **596**, 583–589.
Khan M A, Al Mamun Khan M A, Mahfuz A M U B, Sanjana J M, Ahsan A, Gupta D R, Hoque M N, Islam T. 2022. Highly potent natural fungicides identified in silico against the cereal killer fungus *Magnaporthe oryzae*. *Scientific Reports*, **12**, 20232.
Levesque-Tremblay G, Pelloux J, Braybrook S A, Müller K. 2015. Tuning of pectin methylesterification: Consequences for cell wall biomechanics and development. *Planta*, **242**, 791–811.
Li H, Mo P, Zhang J, Xie Z, Liu X, Chen H, Yang L, Liu M, Zhang H, Wang P, Zhang Z. 2023. Methionine biosynthesis enzyme MoMet2 is required for rice blast fungus pathogenicity by promoting virulence gene expression via reducing 5mC modification. *PLoS Genetics*, **19**, e1010927.
Li J, Hsu H C, Mountz J D, Allen J G. 2018. Unmasking fucosylation: From cell adhesion to immune system regulation and diseases. *Cell Chemical Biology*, **25**, 499–512.
Li W, Zhan P, De Clercq E, Lou H, Liu X. 2013. Current drug research on PEGylation with small molecular agents. *Progress in Polymer Science*, **38**, 421–444.
Li X, Gao C, Li L, Liu M, Yin Z, Zhang H, Zheng X, Wang P, Zhang Z. 2017. MoEnd3 regulates appressorium formation and virulence through mediating endocytosis in rice blast fungus *Magnaporthe oryzae*. *PLoS Pathogens*, **13**, e1006449.
Liu M, Wang F, He B, Hu J, Dai Y, Chen W, Yi M, Zhang H, Ye Y, Cui Z, Zheng X, Wang P, Xing W, Zhang Z. 2024. Targeting *Magnaporthe oryzae* effector MoErs1 and host papain-like protease OsRD21 interaction to combat rice blast. *Nature Plants*, **10**, 618–632.
Liu X, Qian B, Gao C, Huang S, Cai Y, Zhang H, Zheng X, Wang P, Zhang Z. 2016. The putative protein phosphatase MoYvh1 functions upstream of MoPdeH to regulate the development and pathogenicity in *Magnaporthe oryzae*. *Molecular Plant-Microbe Interactions*, **29**, 496–507.
Lu X, Zhang D, Shoji H, Duan C, Zhang G, Isaji T, Wang Y, Fukuda T, Gu J. 2019. Deficiency of α1,6-fucosyltransferase promotes neuroinflammation by increasing the sensitivity of glial cells to inflammatory mediators. *Biochimica et Biophysica Acta-General Subjects*, **1863**, 598–608.
Ma D, Xu J, Wu M, Zhang R, Hu Z, Ji C A, Wang Y, Zhang Z, Yu R, Liu X, Yang L, Li G, Shen D, Liu M, Yang Z, Zhang H, Wang P, Zhang Z. 2024. Phenazine biosynthesis protein MoPhzF regulates appressorium formation and host infection through canonical metabolic and noncanonical signaling function in *Magnaporthe oryzae*. *New Phytologist*, **242**, 211–230.
Mall R, Kaushik R, Martinez Z A, Thomson M W, Castiglione F. 2025. Benchmarking protein language models for protein crystallization. *Scientific Reports*, **15**, 2381.
Min J, Lin D, Zhang Q, Zhang J, Yu Z. 2012. Structure-based virtual screening of novel inhibitors of the uridyltransferase activity of *Xanthomonas oryzae* pv. *oryzae* GlmU. *European Journal of Medicinal Chemistry*, **53**, 150–158.
Miura K, Tsukagoshi T, Hirano T, Nishio T, Hakamata W. 2019. Development of fluorogenic Substrates of α-L-fucosidase useful for inhibitor screening and gene-expression profiling. *ACS Medicinal Chemistry Letters*, **10**, 1309–1313.
Pan Q, Zhang X L. 2025. Roles of core fucosylation modification in immune system and diseases. *Cell Insight*, **4**, 100211.
Paper J M, Scott-Craig J S, Cavalier D, Faik A, Wiemels R E, Borrusch M S, Bongers M, Walton J D. 2013. Alpha-fucosidases with different substrate specificities from two species of *Fusarium*. *Applied Microbiology and Biotechnology*, **97**, 5371–5380.
Qian B, Guo L, Song C, Ji H. 2023. MoMaf1 mediates vegetative growth, conidiogenesis, and pathogenicity in the rice blast fungus *Magnaporthe oryzae*. *Journal of Fungi*, **9**, 106.
Quoc N B, Nguyen N B C. 2017. The role of cell wall degrading enzymes in pathogenesis of *Magnaporthe oryzae*. *Current Protein & Peptide Science*, **18**, 1019–1034.
Schultink A, Liu L, Zhu L, Pauly M. 2014. Structural diversity and function of xyloglucan sidechain substituents. *Plants*, **3**, 526–542.
Skamnioti P, Gurr S J. 2009. Against the grain: Safeguarding rice from rice blast disease. *Trends in Biotechnology*, **27**,141–150.
Talbot N J, Ebbole D J, Hamer J E. 1993. Identification and characterization of MPG1, a gene involved in pathogenicity from the rice blast fungus *Magnaporthe grisea*. *Plant Cell*, **5**, 1575–1590.
Sweigard J A, Chumley F G, Valent B. 1992. Disruption of a *Maanaporthe arisea* cutinase gene. *Molecular and General Genetics* **232**, 183–190.
Wan J, He M, Hou Q, Zou L, Yang Y, Wei Y, Chen X. 2021. Cell wall associated immunity in plants. *Stress Biology*, **1**, 3.
Wan J X, Zhu X F, Wang Y Q, Liu L Y, Zhang B C, Li G X, Zhou Y H, Zheng S J. 2018. Xyloglucan fucosylation modulates *Arabidopsis* cell wall hemicellulose aluminium binding capacity. *Scientific Reports*, **8**, 428.
Wang B H, Ebbole D J, Wang Z H. 2017. The arms race between *Magnaporthe oryzae* and rice: Diversity and interaction of Avr and R genes. *Journal of Integrative Agriculture*, **16**, 2746–2760.
Wang W, Hu T, Frantom P A, Zheng T, Gerwe B, del Amo D S, Garret S, Seidel R D, Wu P. 2009. Chemoenzymatic synthesis of GDP-L-fucose and the Lewis X glycan derivatives. *Proceedings of the National Academy of Sciences of the United States of America*, **106**, 16096–16101.
Yang X, Yan S, Li G, Li Y, Li J, Cui Z, Sun S, Huo J, Sun Y. 2024. Rice-*Magnaporthe oryzae* interactions in resistant and susceptible rice cultivars under panicle blast infection based on defense-related enzyme activities and metabolomics. *PLoS ONE*, **19**, e0299999.
Zhang H F, Islam T, Liu W D. 2022. Integrated pest management programme for cereal blast fungus *Magnaporthe oryzae*. *Journal of Integrative Agriculture*, **21**, 3420–3433.
Zhang L, Paasch B C, Chen J, Day B, He S Y. 2019. An important role of l-fucose biosynthesis and protein fucosylation genes in *Arabidopsis* immunity. *New Phytologist*, **222**, 981–994.
Zhang S L, Wang Y, Hu J M, Cui X Y, Kang X R, Zhao W, Pan Y M. 2025. The N-mannosyltransferase MoAlg9 plays important roles in the development and pathogenicity of *Magnaporthe oryzae*. *Journal of Integrative Agriculture*, **24**, 2266–2284.
Zhao Z, Liu H, Wang C, Xu J R. 2013. Comparative analysis of fungal genomes reveals different plant cell wall degrading capacity in fungi. *BMC Genomics*, **14**, 274.